Steel and Composite Structures, *Vol. 30, No. 3 (2019) 281-292*
DOI: https://doi.org/10.12989/scs.2019.30.3.281

Analysis of critical fluid velocity and heat transfer in temperature-dependent nanocomposite pipes conveying nanofluid subjected to heat generation, conduction, convection and magnetic field

Mohammad Hosein Fakhar, Ahmad Fakhar* and Hamidreza Tabatabaei

Department of Mechanical Engineering, Kashan Branch, Islamic Azad University, Kashan, Iran

(*Received May 21, 2018, Revised July 20, 2018, Accepted January 13, 2019*)

Abstract. In this paper, analysis of critical fluid velocity and heat transfer in the nanocomposite pipes conveying nanofluid is presented. The pipe is reinforced by carbon nanotubes (CNTs) and the fluid is mixed by AL_2O_3 nanoparticles. The material properties of the nanocomposite pipe and nanofluid are considered temperature-dependent and the structure is subjected to magnetic field. The forces of fluid viscosity and turbulent pressure are obtained using momentum equations of fluid. Based on energy balance, the convection of inner and outer fluids, conduction of pipe and heat generation are considered. For mathematical modeling of the nanocomposite pipes, the first order shear deformation theory (FSDT) and energy method are used. Utilizing the Lagrange method, the coupled pipe-nanofluid motion equations are derived. Applying a semi-analytical method, the motion equations are solved for obtaining the critical fluid velocity and critical Reynolds and Nusselt numbers. The effects of CNTs volume percent, AL_2O_3 nanoparticles volume percent, length to radius ratio of the pipe and shell surface roughness were shown on the critical fluid velocity, critical Reynolds and Nusselt numbers. The results are validated with other published work which shows the accuracy of obtained results of this work. Numerical results indicate that for heat generation of Q = 10 MW/m^3, adding 6% AL_2O_3 nanoparticles to the fluid increases 20% the critical fluid velocity and 15% the Nusselt number which can be useful for heat exchangers.

Keywords: critical fluid velocity; nanocomposite pipes; nanofluid; heat generation; temperature-dependent

1. Introduction

The forces induced by fluid and temperature to the pipelines are very important factors in damage and instability of them. However, researchers study different ways to improve the quality and stiffness of the pipelines across the mentioned loads. One of the new and good ways for increasing the stiffness of the structure is using CNTs as reinforce for pipelines since the Yong modulus of CNTs are about 1 TPa. In addition, for improving the heat transfer in the pipelines, mixing the fluid with nanoparticles is a good choice. However, in this paper, we presented the instability and heat transfer in nanocomposite pipelines conveying nanofluid.

Heat transfer in the pipe is reported by several researchers. Chica and Morente (2008) presented a new model for transient heat transfer model on external steel elements. The experimental study was performed by Shi *et al*. (2010) on five eccentric radial heat pipes with two outer-tube diameters. A practical quasi three-dimensional numerical model was developed by Li and Peterson (2011) to investigate the heat and mass transfer in a square flat evaporator of a loop heat pipe with a fully saturated wicking structure. Convective heat transfer phenomenon was investigated by Chandel *et al*. (2012) experimentally as well as numerically in a thick-walled pipe for laminar flow as well turbulent flow. Evaporative heat transfer analysis of a heat pipe with hybrid axial groove was presented by Bai *et al*. (2013). Analysis of a circular pipe heated internally with a cyclic expanding convection boundary condition was performed by Sun and Zhang (2015). Analysis of heat transfer through a high strength concrete with circular pipe in a safety vessel of reactor vault was studied by Anish *et al*. (2017). Moradi-Dastjerdi and Payganeh (2017) studied transient heat transfer analysis of functionally graded (FG) carbon nanotube reinforced nanocomposite (CNTRC) cylinders with various essential and natural boundary conditions. A functionally graded magneto-thermoelastic half space with memory-dependent derivatives heat transfer was presented by Ezzat and El-Bary (2017). To clearly understand the operation phenomena of thermosyphon heat pipes, Kim *et al*. (2017) experimentally investigated the visualization of the operation and limit conditions for a water-filled thermosyphon as well as its thermal performance. Ding *et al*. (2018) presented an experimental study on boiling heat transfer and flow characteristics in a separated heat pipe system. Experiments and numerical simulations were used by Li *et al*. (2018) to study the heat transfer characteristics of a heat exchange system. Single phase heat transfer in a partially-filled, rotating horizontal pipe with axial liquid (water) flow was studied by Chatterjee *et al*. (2018).

In none of the above works, the nanofluid has not been

*Corresponding author, Ph.D.,
E-mail: a.fakhar@iaukashan.ac.ir

http://www.techno-press.org/?journal=scs&subpage=6
ISSN: 1229-9367 (Print), 1598-6233 (Online)

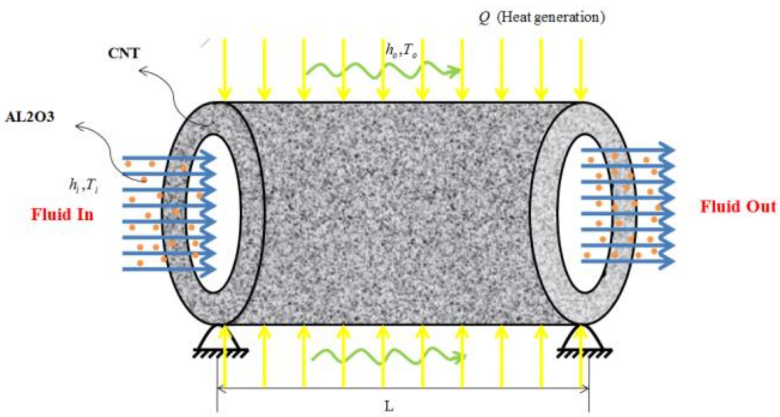

Fig. 1 Schematic figure of pipe reinforced by CNTs conveying AL_2O_3 nanoparticles-fluid flow subjected to heat generation, convection and conduction

used by researchers. Massoudi *et al*. (1999) presented the governing equations for the flow of a dense particulate mixture in a pipe. The governing equations for the individual constituent as well as the mixture were provided based on continuum mechanics. Mixture theory was used by Massoudi and Johnson (2000) to develop a model for a flowing mixture of solid particulates and a fluid. Equations describing the flow of a two-component mixture consisting of a Newtonian fluid and a granular solid were derived. The effect of coal particle size distributions on rheology of coal–water slurries (CWS) was studied by Boylu *et al*. (2004). Experimental results on the steady-state viscosity of carbon nanotubes water-based nanofluids were presented by Halelfadl *et al*. (2013) considering the influence of particle volume fraction and temperature. A water-based TiO_2 nanofluid was studied by Colla *et al*. (2015) in order to evaluate the convective heat transfer under laminar forced and mixedflow conditions. Viscosity and thermal conductivity of the employed nanofluid were nearly identical with the equivalent values of the basefluid water. A numerical investigation of mixed convection was carried out by Al-asadi *et al*. (2017) to study the heat transfer and fluid flow characteristics in an inclined circular pipe using the finite volume method. A numerical investigation was carried out by Saha and Paul (2017) to investigate the transitional flow behaviour of nanofluids flow in an inclined pipe using both single and multi-phase models. Kang *et al*. (2017) studied visualization and thermal resistance measurements for a magnetic nanofluid pulsating heat pipe. In order to examine the laminar convective heat transfer of nanofluid, experiments were conducted by Hussein (2017) using a hybrid nanofluid through a double pipe heat exchanger. The experimental investigation was conducted by Vijayakumar *et al*. (2017) on the heat transfer characteristics of inclined copper sintered wick heat pipes using surfactant free CuO and Al_2O_3 nanofluids.

To the best author's knowledge, no study on instability and heat transfer of nanocomposite pipes conveying nanofluid has been found in the literature. Hence, in this work, a mathematical model is used for nanocomposite pipes conveying nanofluid subjected to heat generation, conduction and convection. The pipe is reinforced by CNTs and the fluid is mixed by AL_2O_3 nanoparticles. The material properties of the nanocomposite pipe and nanofluid are considered temperature-dependent and the structure is subjected to magnetic field. Coupling the momentum equation of the fluid, balance energy of the pipe and FSDT, the motion equations are derived utilizing the Lagrange method. Using a semi-analytical method, the critical fluid velocity and critical Reynolds and Nusselt numbers are obtained. The effects of different parameters such as CNTs volume percent, AL_2O_3 nanoparticles volume percent, length to radius ratio of the pipe and shell surface roughness were shown on the critical fluid velocity, critical Reynolds and Nusselt numbers.

2. Mathematical modeling of structure

In Fig. 1, a pipe reinforced by CNTs conveying AL_2O_3 nanoparticles-fluid flow is shown subjected to heat generation, convection and conduction. The geometrical parameters of the pipe are length L, radius R and thickness h.

The coordinate axis of the pipe is located in the middle surface of left corner with the components of x, θ and z along the axial, circumferential and transverse directions, respectively.

There are many new theories for modeling of different structures. Some of the new theories have been used by Tounsi and co-authors (Bessaim *et al*. 2013, Bouderba *et al*. 2013, Belabed *et al*. 2014, Meziane *et al*. 2014, Zidi *et al*. 2014, Bourada *et al*. 2015, Bousahla *et al*. 2016a, b, Beldjelili *et al*. 2016, Boukhari *et al*. 2016, Draiche *et al*. 2016, Bellifa *et al*. 2015, Attia *et al*. 2015, Mahi *et al*. 2015, Bennoun *et al*. 2016, El-Haina *et al*. 2017, Menasria *et al*. 2017, Chikh *et al*. 2017, Zemri *et al*. 2015, Larbi Chaht *et al*. 2015, Belkorissat *et al*. 2015, Ahouel *et al*. 2016, Bounouara *et al*. 2016, Bouafia *et al*. 2017, Besseghier *et al*. 2017, Bellifa *et al*. 2017, Mouffoki *et al*. 2017, Khetir *et al*. 2017).

In this section, first order shear deformation theory is used. Based on this theory, the displacement field of the pipe can be written as (Reddy 2002)

$$u_x(x,\theta,z,t) = u\ (x,\theta,t) + z\psi_x(x,\theta,t), \qquad (1)$$

$$u_\theta(x,\theta,z,t) = v(x,\theta,t) + z\psi_\theta(x,\theta,t),$$
$$u_z(x,\theta,z,t) = w(x,\theta,t), \tag{1}$$

where (u_x, u_θ, u_z) show the displacement components of any arbitrary point (x, θ, z) in the shell. Also, (u, v, w) denote the displacement of a material point at (x, θ) on the mid-plane (i.e., z = 0) of the shell in direction of the x-, θ-, and z- axes, respectively. Furthermore, ψ_x and ψ_θ indicate the rotations of the normal to the mid-plane about x- and θ- axes, respectively. Using the above relation, the strain-displacement relation can be expressed as

$$\begin{bmatrix}\varepsilon_{xx}\\ \varepsilon_{\theta\theta}\\ \gamma_{\theta z}\\ \gamma_{xz}\\ \gamma_{x\theta}\end{bmatrix} = \begin{bmatrix}\varepsilon^0_{xx}\\ \varepsilon^0_{\theta\theta}\\ \gamma^0_{\theta z}\\ \gamma^0_{xz}\\ \gamma^0_{x\theta}\end{bmatrix} + z\begin{bmatrix}\varepsilon^1_{xx}\\ \varepsilon^1_{\theta\theta}\\ \gamma^1_{\theta z}\\ \gamma^1_{xz}\\ \gamma^1_{x\theta}\end{bmatrix} = \begin{bmatrix}\frac{\partial u}{\partial x} + \frac{1}{2}\left(\frac{\partial w}{\partial x}\right)^2\\ \frac{\partial v}{R\partial\theta} + \frac{w}{R} + \frac{1}{2}\left(\frac{\partial w}{R\partial\theta}\right)\\ \frac{\partial w}{R\partial\theta} - \frac{v}{R} + \psi_\theta\\ \frac{\partial w}{\partial x} + \psi_x\\ \frac{\partial u}{R\partial\theta} + \frac{\partial v}{\partial x} + \frac{\partial w}{\partial x}\frac{\partial w}{R\partial\theta}\end{bmatrix} + z\begin{bmatrix}\frac{\partial\psi_x}{\partial x}\\ \frac{\partial\psi_\theta}{R\partial\theta}\\ 0\\ 0\\ \frac{\partial\psi_x}{R\partial\theta} + \frac{\partial\psi_\theta}{\partial x}\end{bmatrix}. \tag{2}$$

The stress-strain relations of the pipe can be expressed as follows based on Mori-Tanaka model (Shi and Feng 2004)

$$\begin{Bmatrix}\sigma_{xx}\\ \sigma_{\theta\theta}\\ \sigma_{zz}\\ \sigma_{\theta z}\\ \sigma_{xz}\\ \sigma_{x\theta}\end{Bmatrix} = \begin{bmatrix}k+m & l & k-m & 0 & 0 & 0\\ l & n & l & 0 & 0 & 0\\ k-m & l & k+m & 0 & 0 & 0\\ 0 & 0 & 0 & p & 0 & 0\\ 0 & 0 & 0 & 0 & m & 0\\ 0 & 0 & 0 & 0 & 0 & p\end{bmatrix}\begin{Bmatrix}\varepsilon_{xx} - \alpha_{xx}T\\ \varepsilon_{\theta\theta} - \alpha_{\theta\theta}T\\ \varepsilon_{zz}\\ \gamma_{\theta z}\\ \gamma_{xz}\\ \gamma_{x\theta}\end{Bmatrix}, \tag{3}$$

in which k, m, n, l, p represent the stiffness coefficients of the CNTs-reinforced pipe which can be written as

$$\begin{aligned}
k &= \frac{E_m\{E_m c_m + 2k_r(1+\nu_m)[1+c_r(1-2\nu_m)]\}}{2(1+\nu_m)[E_m(1+c_r-2\nu_m)+2c_m k_r(1-\nu_m-2\nu_m^2)]}\\
l &= \frac{E_m\{c_m\nu_m[E_m+2k_r(1+\nu_m)]+2c_r l_r(1-\nu_m^2)]\}}{(1+\nu_m)[E_m(1+c_r-2\nu_m)+2c_m k_r(1-\nu_m-2\nu_m^2)]}\\
n &= \frac{E_m^2 c_m(1+c_r-c_m\nu_m)+2c_m c_r(k_r n_r - l_r^2)(1+\nu_m)^2(1-2\nu_m)}{(1+\nu_m)[E_m(1+c_r-2\nu_m)+2c_m k_r(1-\nu_m-2\nu_m^2)]}\\
&\quad + \frac{E_m[2c_m^2 k_r(1-\nu_m)+c_r n_r(1+c_r-2\nu_m)-4c_m l_r \nu_m]}{E_m(1+c_r-2\nu_m)+2c_m k_r(1-\nu_m-2\nu_m^2)}\\
p &= \frac{E_m[E_m c_m + 2p_r(1+\nu_m)(1+c_r)]}{2(1+\nu_m)[E_m(1+c_r)+2c_m p_r(1+\nu_m)]}\\
m &= \frac{E_m[E_m c_m + 2m_r(1+\nu_m)(3+c_r-4\nu_m)]}{2(1+\nu_m)\{E_m[c_m+4c_r(1-\nu_m)]+2c_m m_r(3-\nu_m-4\nu_m^2)\}}
\end{aligned} \tag{4}$$

where the subscripts m and r are related to matrix and reinforcement, respectively; E_m and v_m are Yong modulus and Poisson's ration of the pipe; k_r, l_r, n_r, p_r, m_r represent the Hills elastic modulus for the CNTs; c_m and c_r denote the volume fractions of the matrix and the nanoparticles, respectively.

2.1 Temperature distribution

The thermal conditions assumed in this paper are, the convection of inside fluid in the pipe, convection of outer air over the pipe, the conduction of the pipe in the thickness direction and the constant heat generation ($\dot{q}$). Based on the mentioned assumptions, the energy balance equation in the (x, θ, z) coordinate can be simplified as follows

$$\frac{d^2T}{dz^2} + \frac{\dot{q}}{k_e} = 0, \tag{5}$$

Solution of the above relation yields

$$T = -\frac{Qz^2}{2k_e} + \mathrm{C}_1 z + \mathrm{C}_2, \tag{6}$$

The boundary conditions are

$$z = -\frac{h}{2} @ k_e\frac{\partial T}{\partial z} = -h_i\left(T_i - T\right), \tag{7}$$

$$z = \frac{h}{2} @ k_e\frac{\partial T}{\partial z} = h_o\left(T_o - T\right) + \mathrm{Q}, \tag{8}$$

where h_i and h_o are convective heat transfer coefficients in the inner and outer fluids, respectively; T_i and T_o are temperature of the inner and outer fluids, respectively; Q is heat source. Noted that the temperature of the fluid can be obtained by the energy equation (Eq. (13)).

2.2 Energies of the pipe

The potential energy of the pipe can be presented as follows

$$U_P = \frac{1}{2}\int_0^{2\pi}\int_0^L\int_{-h/2}^{h/2}\begin{pmatrix}\sigma_{xx}\varepsilon_{xx} + \sigma_{\theta\theta}\varepsilon_{\theta\theta} + \sigma_{x\theta}\gamma_{x\theta}\\ +\sigma_{xz}\gamma_{xz} + \sigma_{\theta z}\gamma_{\theta z}\end{pmatrix} dz dx R d\theta. \tag{9a}$$

The kinetic energy of the pipe can be expressed as follows

$$T_P = \frac{\rho_P}{2}\int_0^{2\pi}\int_0^L\int_{-h/2}^{h/2}\left(\left(\frac{\partial u_x}{\partial t}\right)^2 + \left(\frac{\partial u_\theta}{\partial t}\right)^2 + \left(\frac{\partial u_z}{\partial t}\right)^2\right) dz dx R d\theta. \tag{9b}$$

The external work in the pipe can be expressed as follows

$$W_P = \int_0^{2\pi}\int_0^L\left(\eta H_x^2\frac{\partial^2 w}{\partial x^2} + \frac{N_x^T}{2}\left(\frac{\partial w}{\partial x}\right)^2 + \frac{N_\theta^T}{2}\left(\frac{\partial w}{R\partial\theta}\right)^2\right) dx R d\theta, \tag{10}$$

where η and H_x are magnetic permeability and magnetic field, respectively; N_x^T and N_θ^T are thermal forces in the axial and circumferential directions, respectively.

3. Fluid–structure interaction

In this section, the cylindrical coordinates r, θ and z is used with the origin located at the center of shell's section. With the assumption of Newtonian fluid, steady state, incompressible flow and turbulent flow regime, the governing equations for the fluid are as follows:

Continuity

$$\frac{1}{r}\frac{\partial v_r}{\partial r}+\frac{\partial v_\theta}{r\partial\theta}+\frac{\partial v_x}{\partial x}=0 \tag{11}$$

Momentum

$$\begin{aligned}&v_x\frac{\partial v_x}{\partial x}+v_r\frac{\partial v_x}{\partial r}+\frac{v_\theta}{r}\frac{\partial v_x}{\partial\theta}=-\frac{1}{\rho_e}\frac{\partial P}{\partial x}\\&-\left(\frac{\partial}{\partial x}(\bar{v}_x)^2+\frac{1}{r}\frac{\partial}{\partial r}r\bar{v}_x\bar{v}_r+\frac{1}{r}\frac{\partial}{\partial\theta}\bar{v}_x\bar{v}_\theta\right)+\frac{\mu_e}{\rho_e}\nabla^2 v_x\end{aligned} \tag{12}$$

$$\begin{aligned}&v_x\frac{\partial v_r}{\partial x}+v_r\frac{\partial v_r}{\partial r}+\frac{v_\theta}{r}\frac{\partial v_r}{\partial\theta}-\frac{(v_\theta)^2}{r}=\\&-\frac{1}{\rho_e}\frac{\partial P}{\partial r}-\left(\frac{\partial}{\partial x}\bar{v}_x\bar{v}_r+\frac{1}{r}\frac{\partial}{\partial r}r(\bar{v}_r)^2\right.\\&\left.+\frac{1}{r}\frac{\partial}{\partial\theta}\bar{v}_r\bar{v}_\theta-\frac{(\bar{v}_\theta)^2}{r}\right)+\frac{\mu_e}{\rho_e}\left(\nabla^2 v_r-\frac{v_r}{r^2}-\frac{2}{r^2}\frac{\partial v_\theta}{\partial\theta}\right)\end{aligned} \tag{13}$$

$$\begin{aligned}&v_x\frac{\partial v_\theta}{\partial x}+v_r\frac{\partial v_\theta}{\partial r}+\frac{v_\theta}{r}\frac{\partial v_\theta}{\partial\theta}-\frac{v_\theta v_r}{r}=\\&-\frac{1}{r\rho_e}\frac{\partial P}{\partial\theta}-\left(\frac{\partial}{\partial x}\bar{v}_x\bar{v}_\theta+\frac{\partial}{\partial r}\bar{v}_\theta\bar{v}_r\right.\\&\left.+\frac{1}{r}\frac{\partial}{\partial\theta}(\bar{v}_\theta)^2-\frac{2\bar{v}_r\bar{v}_\theta}{r}\right)+\frac{\mu_e}{\rho_e}\left(\nabla^2 v_\theta-\frac{v_\theta}{r^2}+\frac{2}{r^2}\frac{\partial v_\theta}{\partial\theta}\right)\end{aligned} \tag{14}$$

Energy

$$\begin{aligned}&\frac{\partial T}{\partial t}+v_r\frac{\partial T}{\partial r}+v_\theta\frac{\partial T}{r\partial\theta}+v_x\frac{\partial T}{\partial x}=\\&\frac{k_e}{c_{pe}\rho_e}\left(\frac{1}{r}\frac{\partial}{\partial r}\left(r\frac{\partial T}{\partial r}\right)+\frac{\partial^2 T}{r^2\partial\theta^2}+\frac{\partial^2 T}{\partial x^2}\right),\end{aligned} \tag{15}$$

where $\overline{v_r}$, $\overline{v_\theta}$, $\overline{v_x}$ are the turbulent fluctuating velocity components in the r , θ and x directions, respectively; T is the temperature distribution; k_e, c_{pe}, ρ_e and μ_e are the thermal conductivity, heat capacity, density and fluid viscosity of the AL_2O_3-water nanofluid, respectively which can be expressed as (Buongiorno 2006, Maiga *et al*. 2005, Nguyen *et al*. 2007, Khanafer and Vafai 2011)

$$\rho_e=(1-\phi)\rho_f+\phi\rho_p, \tag{16}$$

$$c_{pe}=\frac{(1-\phi)\rho_f c_f+\phi\rho_p c_p}{\rho_e}, \tag{17}$$

$$\mu_e=\left(1+39.11\phi+533.9\phi^2\right)\mu_f, \tag{18}$$

$$\begin{aligned}&\frac{k_e}{k_f}=0.9843+0.398\phi^{0.7383}\left(\frac{1}{d_p}\right)^{0.2246}\\&\left(\frac{\mu_e}{\mu_f}\right)^{0.0235}-3.9517\frac{\phi}{T}+34.034\frac{\phi^2}{T^3}+32.509\frac{\phi}{T^2},\end{aligned} \tag{19}$$

where ϕ and d_p are AL_2O_3 volume percent and diameter in nano meter dimension, respectively; T is in Celsius. The viscosity of water in different temperatures is obtained by

$$\mu_f=2.414\times10^{-5}\times10^{\frac{247.8}{T-140}} \tag{20}$$

where T is in Kelvin.

3.1 Fluid viscosity forces

In a fully developed turbulent pipe flow, $v_r=v_\theta=0$, $\frac{\partial}{\partial 0}=0$ and the velocity field is independent of the coordinate x. With the mentioned simplification, the time-mean Navier–Stokes equations can be expressed as (Paak *et al*. 2014)

$$\frac{1}{\rho_e}\frac{\partial P}{\partial x}=-\frac{1}{r}\frac{\partial}{\partial r}\left(r\bar{v}_x\bar{v}_r\right)+\frac{\mu_e}{r\rho_e}\frac{d}{dr}\left(r\frac{dv_x}{dr}\right), \tag{21}$$

$$\frac{1}{\rho_e}\frac{\partial P}{\partial r}=-\frac{1}{r}\frac{\partial}{\partial r}r(\bar{v}_r)^2+\frac{(\bar{v}_\theta)^2}{r}, \tag{22}$$

$$0=-\frac{\partial}{\partial r}\bar{v}_\theta\bar{v}_r-\frac{2\bar{v}_r\bar{v}_\theta}{r}, \tag{23}$$

After lengthy mathematical manipulations, the pressure distribution can be written as

$$\begin{aligned}&\bar{p}(\mathrm{x,r})=-2\frac{\rho_e}{R}U_\tau^2 x-\rho_e(\bar{v}_r)^2+\\&\rho_e\int_R^r\frac{(\bar{v}_\theta)^2-(\bar{v}_r)^2}{r}dr+\bar{p}(0,R),\end{aligned} \tag{24}$$

where U_τ is the shear velocity which can be defined as

$$U_\tau^2=\left(\frac{\mu_e}{\rho_e}\right)\left(\frac{dv_x}{dr}\right)\Bigg|_{r=R}=\frac{\tau_w}{\rho_e}=\left(\frac{1}{8}fv_x^2\right), \tag{25}$$

where τ_w is the fluid frictional force per unit area on the pipe and f is the Darcy friction factor which may be calculated using Colebrook's implicit expression as follows (White 1986)

$$\frac{1}{\sqrt{f}}=-2\log_{10}\left(\frac{\varepsilon/D}{3.7}+\frac{2.51}{\mathrm{Re}\sqrt{f}}\right), \tag{26}$$

where ε, D and Re are respectively, pipe surface roughness, pipe diameter and Reynolds number. The initial value for f can be obtained from the following relation

$$\frac{1}{\sqrt{f}}=-1.8\log_{10}\left(\left(\frac{\varepsilon/D}{3.7}\right)^{1.11}+\frac{6.9}{\mathrm{Re}}\right), \tag{27}$$

The distribution of mean pressure inside the pipe can be written as

$$P_r=2\frac{\rho_e}{R}U_\tau^2L, \tag{28}$$

$$P_x=\rho_eU_\tau^2, \tag{29}$$

The work done due to viscosity effect can be expressed as

$$W_{FV}=\int_0^{2\pi}\int_0^L\left(P_rw+P_xu\right)dxRd\theta. \tag{30}$$

3.2 Perturbation pressure

The fluid structure interaction is described by linear potential flow theory. The flow velocity V may be expressed as (Amabili *et al*. 2009)

$$\boldsymbol{V}=-\nabla\Psi, \tag{31}$$

where ψ is a potential function including two components due to mean undisturbed flow velocity v_x and the shell motions. Hence

$$\Psi=-v_xx+\Phi, \tag{32}$$

The potential of the unsteady component Φ satisfies the Laplace equation

$$\nabla^2\Phi=\frac{\partial^2\Phi}{\partial x^2}+\frac{\partial^2\Phi}{\partial r^2}+\frac{1}{r}\frac{\partial\Phi}{\partial r}+\frac{1}{r^2}\frac{\partial\Phi}{\partial\theta^2}=0, \tag{33}$$

In order to obtain the perturbed pressure (P) in term of velocity potential, the Bernoulli's equation is used as

$$-\frac{\partial\Phi}{\partial t}+\frac{1}{2}V^2+\frac{\bar{P}+p}{\rho_e}=\frac{\bar{P}+1/2\rho_f\left(v_x\right)^2}{\rho_e}, \tag{34}$$

where $\bar{P}$ and p are the mean pressure and perturbation pressure, respectively and for small perturbations we have

$$V^2=\left(v_x\right)^2-2v_x\frac{\partial\Phi}{\partial x}, \tag{35}$$

However, combining Eqs. (34) and (35) yields the perturbation pressure as follows

$$p=\rho_e\left(\frac{\partial\Phi}{\partial t}+v_x\frac{\partial\Phi}{\partial x}\right) \tag{36}$$

Assuming that there is no cavitation at the fluid-pipe interface, the boundary condition between the pipe wall and the flow is

$$\left(\frac{\partial\Phi}{\partial r}\right)_{r=R}=\left(\frac{\partial w}{\partial t}+v_x\frac{\partial w}{\partial x}\right), \tag{37}$$

in which w is the transverse deflection of the structure. Using the method of variables separation for Φ, we have

$$\Phi(\mathrm{x},\mathrm{r},\theta,\mathrm{t})=\sum_{m=1}^{M}\sum_{n=0}^{N}\Phi_m(\mathrm{x})\psi_{m,n}(\mathrm{r})\cos(\mathrm{n}\,\theta)\,\mathrm{f}_{m,n}(\mathrm{t}), \tag{38}$$

Substituting Eq. (38) into Eq. (33) and assuming regularity condition at r = 0 for the for potential of perturbation velocity yields

$$\begin{aligned}\Phi_m&=\sin\left(\frac{m\pi x}{L}\right),\\ \psi_{m,n}(\mathrm{r})&=I_n\left(\frac{m\pi r}{L}\right),\end{aligned} \tag{39}$$

where I_n is the first kind modified Bessel function in the order of n. Combining Eqs. (38) and (39) yields

$$\Phi(\mathrm{x},\mathrm{r},\theta,\mathrm{t})=\sum_{m=1}^{M}\sum_{n=0}^{N}\frac{L}{m\pi}\frac{I_n(m\pi r/L)}{I_n^{'}(m\pi R/L)}\left(\frac{\partial w}{\partial t}+v_x\frac{\partial w}{\partial x}\right), \tag{40}$$

in which I_n' is first derivative of I_n.

3.3 Energies of the fluid flow

Based on Green's theorem, the total energy of the fluid flow can be expressed as

$$\begin{aligned}E_F^T&=\frac{1}{2}\rho_e\iiint_\Gamma\vec{V_f}.\vec{V_f}\,d\Gamma=\frac{1}{2}\rho_e\iiint_\Gamma\nabla\Psi.\nabla\Psi\,d\Gamma\\&=\frac{1}{2}\rho_e\iiint_\Gamma\left(\Psi\frac{\partial\Psi}{\partial\chi}\right)\bigg|_\Upsilon d\Upsilon,\end{aligned} \tag{41}$$

where Γ is the cylindrical fluid volume inside the shell; Υ is the boundary surface of this volume; χ is the coordinate along the normal to the boundary which is positive outward. Integrating Eq. (41) on the three main surfaces yields

$$\begin{aligned}E_F^T&=\frac{1}{2}\rho_e\int_0^{2\pi}\int_0^L\left(\Psi\frac{\partial\Psi}{\partial r}\right)_{r=R}dxRd\theta\\&+\frac{1}{2}\rho_e\int_0^{2\pi}\int_0^R\left(\Psi\frac{\partial\Psi}{\partial x}\right)_{x=L}rdrd\theta\\&-\frac{1}{2}\rho_e\int_0^{2\pi}\int_0^R\left(\Psi\frac{\partial\Psi}{\partial x}\right)_{x=0}rdrd\theta,\end{aligned} \tag{42}$$

Using Eqs. (32), Eq. (42) can be expressed as

$$\begin{aligned}E_F^T&=\frac{1}{2}\rho_e\int_0^{2\pi}\int_0^L\left(\Phi\frac{\partial\Phi}{\partial r}\right)_{r=R}dxRd\theta\\&+\frac{1}{2}\rho_e\int_0^{2\pi}\int_0^L\left(v_xx\frac{\partial\Phi}{\partial r}\right)_{r=R}dxRd\theta\end{aligned} \tag{43}$$

$$+\frac{1}{2}\rho_e\int_0^{2\pi}\int_0^R\left(v_x x\frac{\partial\Phi}{\partial x}\right)_{x=L} rdrd\theta \\ +\frac{1}{2}\rho_e v_x^2\pi R^2 L, \tag{43}$$

Based on Amabili *et al*. (2009), the second, third and forth terms of above relation can be neglected. However, substituting Eq. (43) into Eq. (43) yields

$$E_F^T=\frac{1}{2}\rho_e\int_0^{2\pi}\int_0^L\left\{\sum_{m=1}^{M}\sum_{n=0}^{N}\frac{L}{m\pi}\frac{I_n(m\pi r/L)}{I_n^{'}(m\pi R/L)}\right. \\ \left.\left(\left(\frac{\partial w}{\partial t}\right)^2+v_x\left(\frac{\partial w}{\partial x}\frac{\partial w}{\partial t}\right)+v_x^2\left(\frac{\partial w}{\partial t}\right)^2\right)\right\}dxRd\theta, \tag{44}$$

The above equation can be distinguished into the three following terms

$$E_F^T=T_F+\mathrm{E}_G-U_F, \tag{45}$$

where T_F, E_G and V_F are kinetic, gyroscopic and potential energies of the fluid flow which can be expressed as follows

$$T_F=\frac{1}{2}\rho_e\int_0^{2\pi}\int_0^L\left\{\sum_{m=1}^{M}\sum_{n=0}^{N}\frac{L}{m\pi}\frac{I_n(m\pi r/L)}{I_n^{'}(m\pi R/L)}\left(\frac{\partial w}{\partial t}\right)^2\right\}dxRd\theta, \tag{46}$$

$$E_G=\frac{1}{2}\rho_e\int_0^{2\pi}\int_0^L\left\{\sum_{m=1}^{M}\sum_{n=0}^{N}\frac{L}{m\pi}\frac{I_n(m\pi r/L)}{I_n^{'}(m\pi R/L)}\right. \\ \left.\left(v_x\left(\frac{\partial w}{\partial x}\frac{\partial w}{\partial t}\right)\right)\right\}dxRd\theta, \tag{47}$$

$$U_F=\frac{1}{2}\rho_e\int_0^{2\pi}\int_0^L\left\{\sum_{m=1}^{M}\sum_{n=0}^{N}\frac{L}{m\pi}\frac{I_n(m\pi r/L)}{I_n^{'}(m\pi R/L)}\right. \\ \left.\left(v_x^2\left(\frac{\partial w}{\partial t}\right)^2\right)\right\}dxRd\theta, \tag{48}$$

4. Motion equations and solution

The motion equations can be derived based on Lagrange equations as follows

$$\frac{d}{dt}\left[\frac{\partial(T_P+T_F+E_G)}{\partial\dot{q}_k}\right]-\frac{\partial(T_P+T_F+E_G)}{\partial q_k} \\ +\frac{\partial(U_P+U_F)}{\partial q_k}=\frac{\partial(W_{FV}+W_P)}{\partial q_k},\ k=1,..,\mathrm{H} \tag{49}$$

where $\{q\}$ is degree of freedoms (DOFs) and H is dimension of vector $\{q\}$ which may be calculated as $H = N^{DOF} + M$. Assuming simply supported boundary conditions at the both ends of the pipe, the mode expansions can be expressed as follows (Amabili *et al*. 2009)

$$\{q\}=\sum_{m=1}^{M}\sum_{n=0}^{N}\sin\left(\frac{(2\mathrm{m}-1)\pi x}{L}\right)\left[\{q_{mn}^c\}\cos(\mathrm{n}\theta)+\{q_{mn}^s\}\sin(\mathrm{n}\theta)\right], \tag{50}$$

in which m and n are longitudinal half wave number and circumferential wave number, respectively; M and N are maximum value of wave numbers;

$\{q\}=\{u_{mn}^c,\ u_{mn}^s,\ v_{mn}^c,\ v_{mn}^s,\ w_{mn}^c,\ w_{mn}^s,\ \psi_{xmn}^c,\ \psi_{xmn}^s,\ \psi_{\theta mn}^c,\psi_{\theta mn}^s\}$ are time-dependent DOFs.

5. Numerical results and discussion

In this section, a pipe with the length to radius ration of $L/R = 4$, thickness to radius of $h/R = 0.02$ is considered. The pipe is made from Poly methyl methacrylate (PMMA) with constant Poisson's ratios of $v_m = 0.34$, temperature-dependent thermal coefficient of $\alpha_m = (1 + 0.0005T) \times 10^{-6}/K$, and temperature-dependent Young moduli of $E_m = (3.52 - 0.0034T)$ GPa in which $T = T_0 + \Delta T$ and $T_0 = 300\ K$ (room temperature) (Kolahchi *et al*. 2016). In addition, the pipe is reinforced by CNTs with the Hill's constants of $k_r = 30$ GPa, $l_r = 10$ GPa, $m_r = 1$ GPa, $n_r = 450$ GPa and $p_r = 30$ GPa (Shi and Feng 2004). The inside fluid is water mixed by AL_2O_3 nanoparticles with the thermo-physical properties listed in Table 1 (Sheikhzadeh *et al*. 2013).

5.1 Temperature distribution

The temperature distribution in the thickness direction of the pipe is shown in Fig. 2. As can be seen, the temperature in the outer surface of the pipe is higher than the inner one since the heat generation source is in the outer surface of the pipe.

5.2 Defining the critical fluid velocity

In Figs. 3(a) and (b), the imaginary and real parts of

Table 1 Thermophysical properties of water and AL_2O_3 nanoparticles

	k (W/mK)	c_p (J/kg K)	ρ (kg/m^3)	T (K)
Water	0.59	4182	998.2	293
AL_2O_3	0.85	765	3970	293

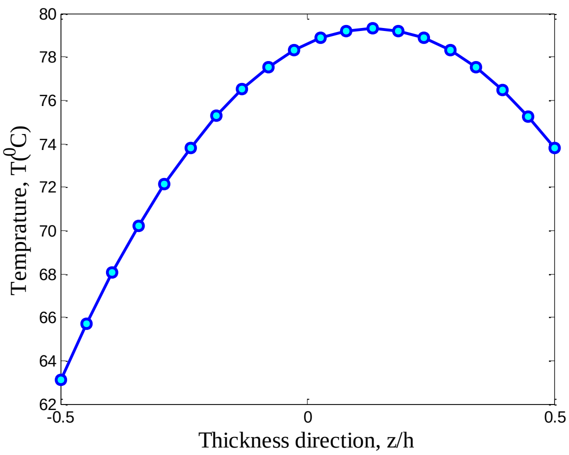

Fig. 2 The temperature distribution in the thickness direction of the pipe

eigenvalue versus fluid are shown. The imaginary and real parts of eigenvalue are frequency (Im(Ω)) and damping (Re(Ω)) of the structure, respectively. As can be seen, frequency decreases with increasing fluid velocity, while the damping remains zero. These imply that the system is stable. When the frequency becomes zero, critical velocity is reached, which the system loses its stability due to the divergence via a pitchfork bifurcation. Hence, the Re(Ω) have the positive real parts, which the system becomes unstable. In this state, both real and imaginary parts of frequency become zero at the same point. In this point (critical fluid velocity), the critical Reynolds ($Re = \rho_e v_x D / \mu_e$) and Nusselt numbers can be happened. In this paper, the Nusselt number is calculated by $St\, Pr^{2/3} = f / 8$ where St and Pr are Stanton and Prandtl numbers, respectively.

5.3 Validation

At the first for results validation of this work, the Al_2O_3 nanoparticles and CNTs as well as thermal load are neglected and the critical fluid velocity in a pipe conveying fluid is studied. The structure parameters of the classical shell assumed as $h/R = 0.01$, $L/R = 2$, $E = 206$ GPa, $\nu = 0.3$, $\rho = 7850$ Kg/m^3 and the water density $\rho_f = 1000$ Kg/m^3. A non-dimensional fluid velocity is defined as $u_f = V/\{\pi^2/L[D/\rho h]\}^{0.5}$, with $D = Eh^3/[12(1-\nu^2]$, and a non-

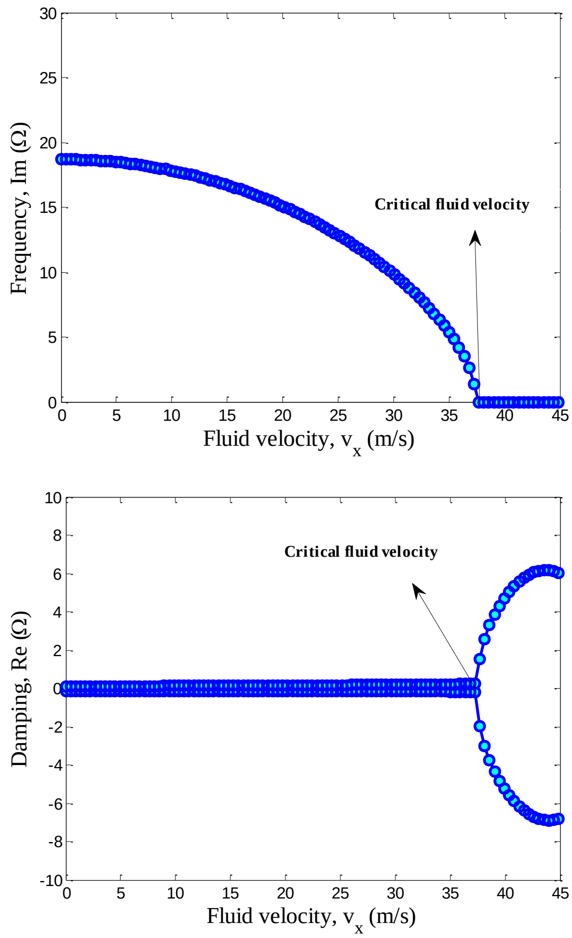

Fig. 3 (a) Imaginary part of frequency versus flow velocity; (b) Real part of frequency versus flow velocity

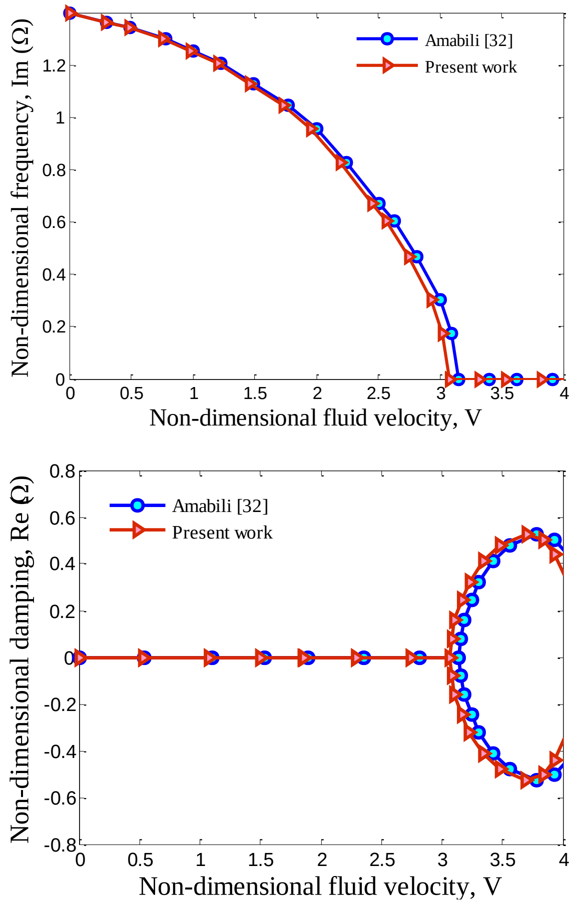

Fig. 4 (a) Imaginary part of frequency versus dimensionless flow velocity; (b) Real part of frequency versus dimensionless flow velocity

dimensional eigenvalue is also defined as $\omega = \lambda/\{\pi^2/L^2[D/\rho h]\}^{0.5}$, where λ is the eigenvalue. Figs. 4(a) and (b) illustrate the imaginary and real parts of frequency versus dimensionless flow velocity, respectively. As can be seen, the obtained results are close with the results of Amabili (2008), indicating validation of our work.

5.4 The effect of different parameters

The effect of CNTs volume percent on the critical fluid velocity, critical Reynolds number and critical Nusselt number is shown in Figs. 5(a)-(c), respectively as a function of heat generation. As can be seen, with increasing the heat generation, the critical fluid velocity is decreased about 49% since the stiffness of the structure reduces and in lower fluid velocity, the pipe becomes unstable. With respect to the direct relation between Reynolds number and fluid velocity, the critical Reynolds number is also decreased with increasing the heat generation value. In addition, the Nusselt number has a direct relation with the Reynolds number. Hence, with decreasing the critical Reynolds number, the critical Nusselt number is also declining. It also concluded that the critical fluid velocity, critical Reynolds number and critical Nusselt number of the pipe without CNTs as reinforce ($c_r = 0$) are higher than those of the nanocomposite pipe ($c_r \neq 0$). In other words, with increasing the CNTs volume percent, the critical fluid velocity, critical Reynolds number and critical Nusselt number will be increased. In other words, for heat generation of Q = 10 MW/m^3, reinforcing the pipe with 0.04% CNTs, the critical fluid velocity improves about 25% which means the instability will be happened at higher fluid velocity. In addition, the critical Nusselt number and consequently the heat transfer are increased about 20% with adding 0.04% CNTs to the pipe which is very useful in heat exchanges.

The critical fluid velocity, critical Reynolds number and critical Nusselt number are presented in Figs. 6(a)-(c), respectively versus the heat generation for different AL_2O_3 nanoparticles volume percents. The critical fluid velocity, critical Reynolds number and critical Nusselt number for Q = 0 and ϕ = 6% are respectively, 46.48 m/s, 1.925e6 and 3572 while these values for Q = 50 MW/m^3 are respectively, 23.74 m/s, 0.98e6 and 2087. This means that with applying heat generation of Q = 50 MW/m^3, the

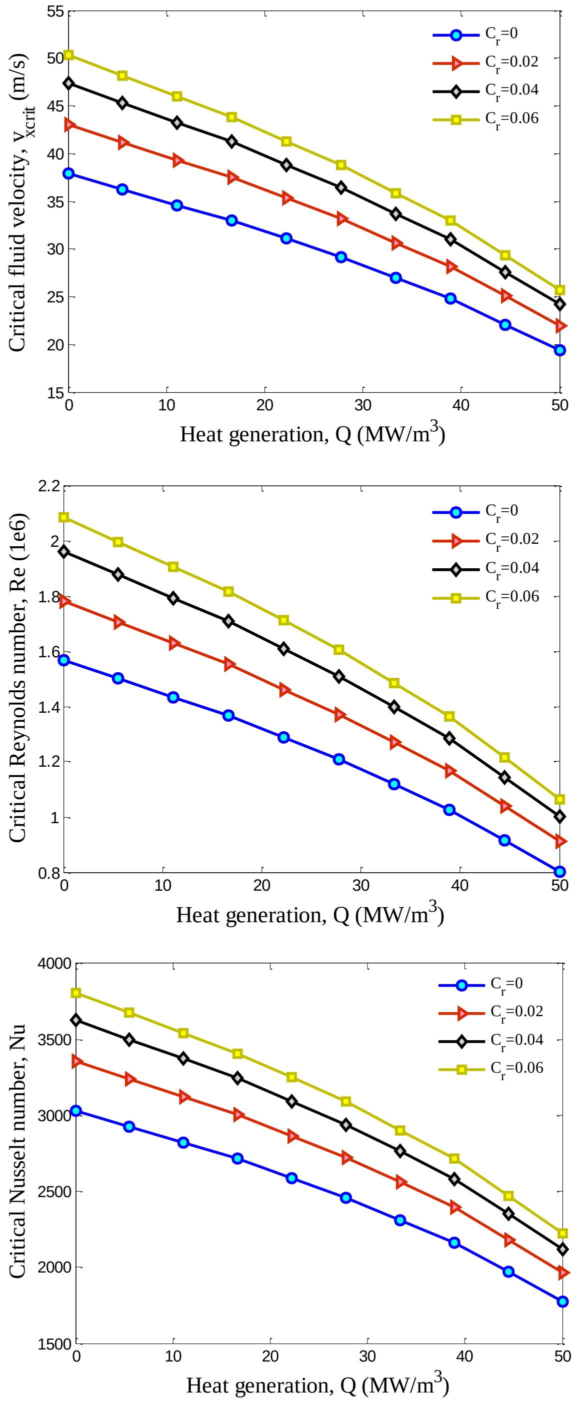

Fig. 5 The effect of heat generation and CNTs volume percent on the (a) critical fluid velocity; (b) critical Reynolds number; (c) critical Nusselt number

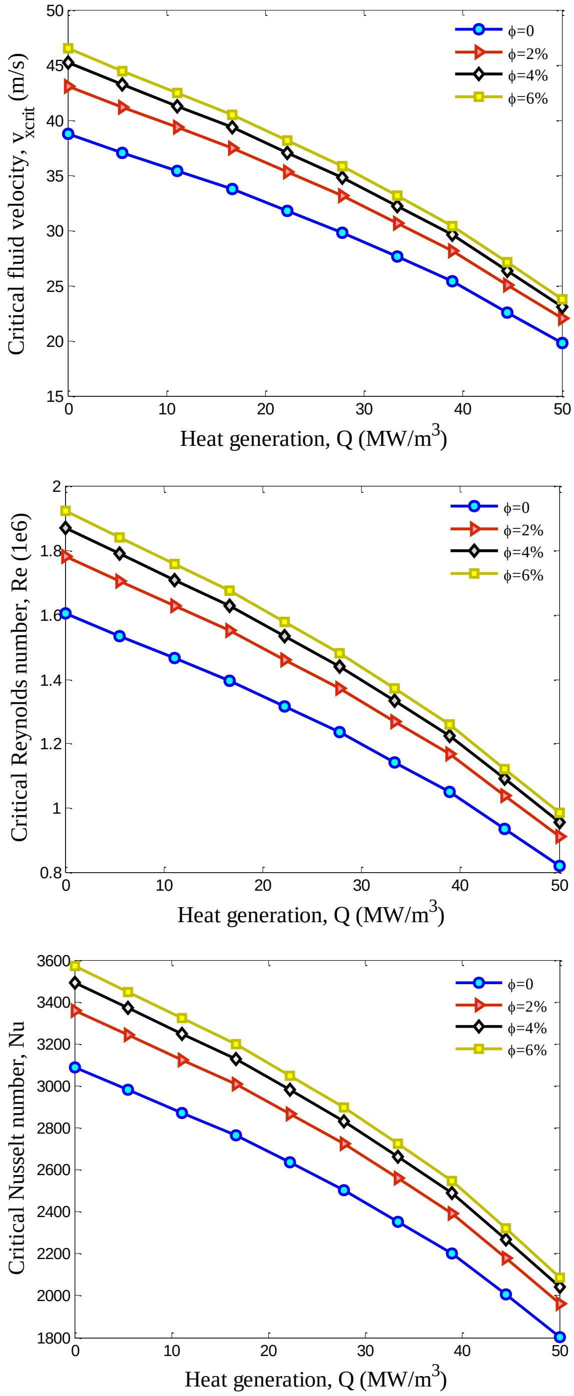

Fig. 6 The effect of heat generation and AL_2O_3 nanoparticles volume percent on the (a) critical fluid velocity; (b) critical Reynolds number; (c) critical Nusselt number

critical fluid velocity, critical Reynolds number and critical Nusselt number are decreased about 49%, 49% and 41%. This is physically reasonable since applying heat generation leads to lower stiffness in the pipe and consequently, the pipe becomes instable at lower fluid velocities. About the effect of AL_2O_3 nanoparticles volume percent, it should be noted that with increasing the AL_2O_3 nanoparticles volume percent in the fluid, the critical fluid velocity, critical Reynolds number and critical Nusselt number increase. In other words, the critical fluid velocity, critical Reynolds number and critical Nusselt number for the fluid without the nanoparticles are 35.39 m/s, 1.466e6 and 2872 while these values are 42.47 m/s, 1.759e6 and 3323, respectively. Consequently, adding 6% AL_2O_3 nanoparticles to the fluid increases 20% the critical fluid velocity and 15% the Nusselt number. It physically means that the AL_2O_3 nanoparticles improve the heat transfer in the fluid which can be useful for heat exchangers.

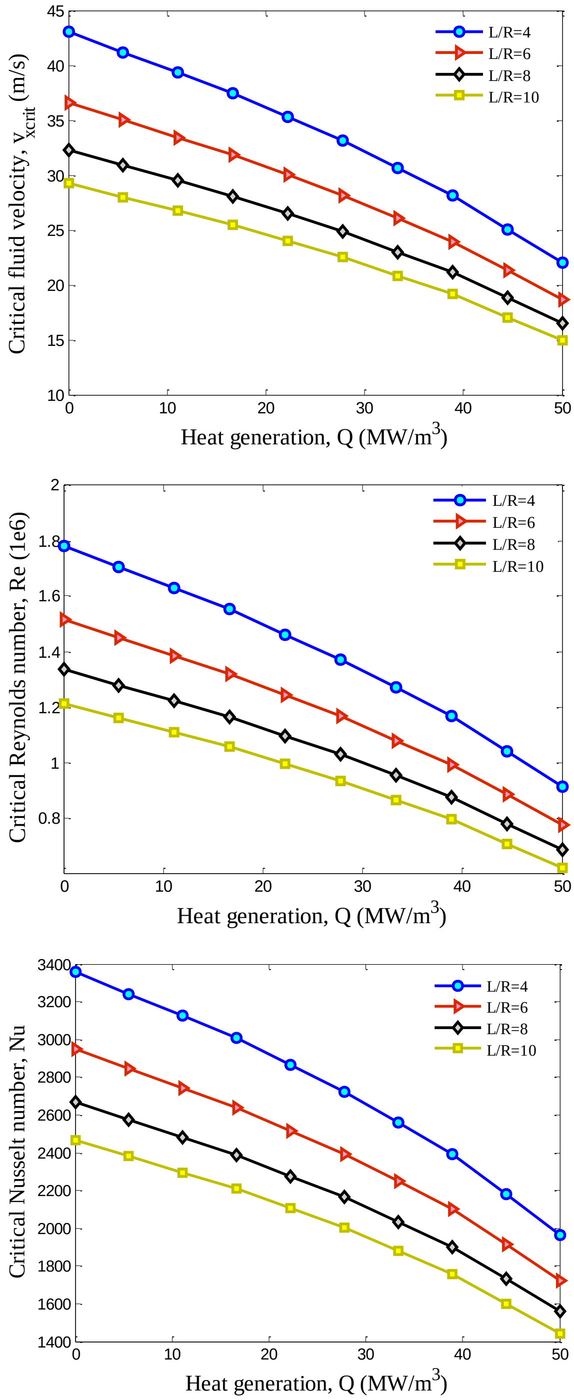

Fig. 7 The effect of heat generation and length to radius ratio of pipe on the (a) critical fluid velocity; (b) critical Reynolds number; (c) critical Nusselt number

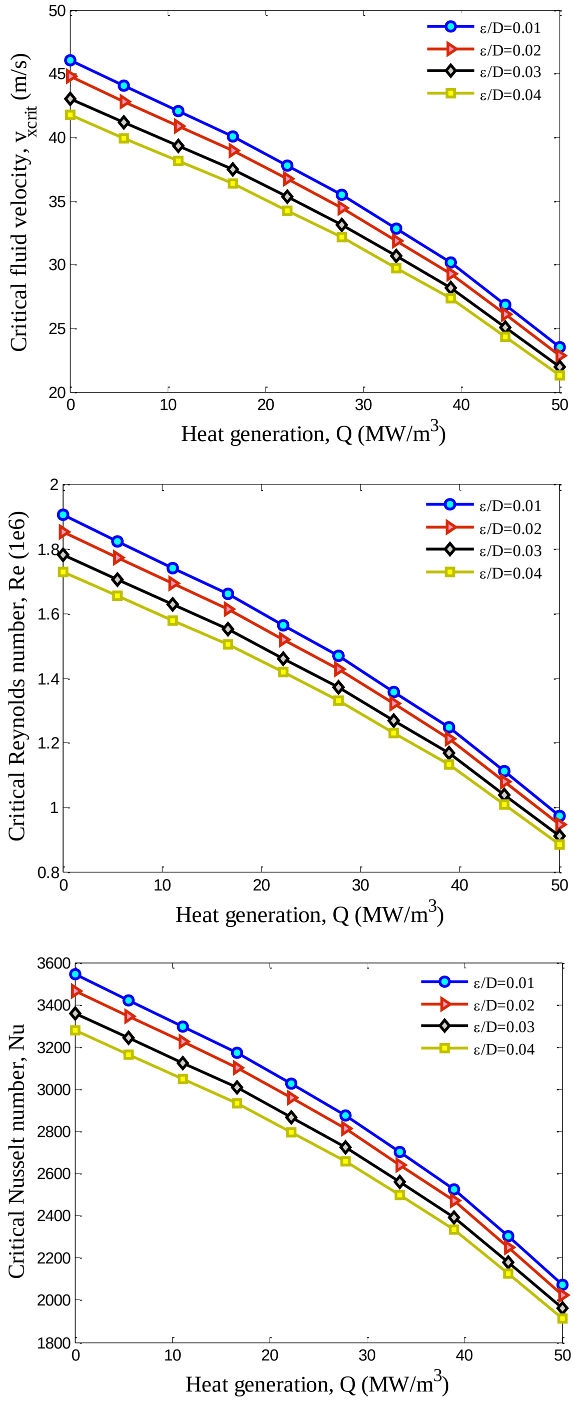

Fig. 8 The effect of heat generation and shell surface roughness to diameter ratio of pipe on the (a) critical fluid velocity; (b) critical Reynolds number; (c) critical Nusselt number

Figs. 7(a)-(c) illustrate the effect of length to radius ratio of the pipe on the critical fluid velocity, critical Reynolds number and critical Nusselt number, respectively versus the heat generation. It can be seen that with increasing the length to radius ratio of the pipe, the critical fluid velocity, critical Reynolds number and critical Nusselt number are decreased. This is due to this fact that with raising the length to radius ratio of the pipe, the stiffness of the pipe decreases and consequently, the pipe will be unstable at lower fluid velocities. Furthermore, with enhancing the length to radius ratio of the pipe, the heat transfer in the pipe decreases.

The effects of shell surface roughness to diameter ratio and heat generation are shown on the critical fluid velocity, critical Reynolds number and critical Nusselt number, respectively. It can be seen that as the shell surface roughness to diameter ratio increases, the critical fluid velocity decreases and the pipe becomes instable at higher fluid velocities. In addition, with raising the shell surface roughness to diameter ratio, the critical Nusselt number decreases and consequently the heat transfer of the inside fluid is declined.

6. Conclusions

Instability of the nanocomposite pipes conveying nanofluid was presented in this paper subjected to thermal loads. The pipe was reinforced by CNTs and the fluid was mixed by AL_2O_3 nanoparticles. The structure was subjected to convection of inner fluid, convection of outer fluid, conduction of the pipe and heat generation. The material properties of the pipes were assumed temperature-dependent and structure was subjected to magnetic field. The inner fluid was considered turbulent and the forces of the viscosity and turbulent pressure were taken into account using momentum equations of the fluid. For modeling of the pipe, the FSDT theory in conjunction with energy method was used. In order to couple the equation of the nanofluid and nanocomposite pipe, the Lagrange method was used. Based on semi-analytical method, the critical fluid velocity and critical Reynolds and Nusselt numbers were calculated. The effects of CNTs volume percent, AL_2O_3 nanoparticles volume percent, length to radius ratio of the pipe and shell surface roughness were shown on the critical fluid velocity and Reynolds and Nusselt numbers. The most findings of this paper were:

- With increasing the heat generation, the critical fluid velocity was decreased about 49% since the stiffness of the structure reduces and in lower fluid velocity, the pipe becomes unstable.
- For heat generation of Q = 10 MW/m^3, With increasing the CNTs volume percent, the critical fluid velocity and critical Reynolds number as well as critical Nusselt number will be increased about 25% and 29%, respectively.
- Adding 6% AL_2O_3 nanoparticles to the fluid increases 20% the critical fluid velocity and 15% the Nusselt number.
- With increasing the length to radius ratio of the pipe, the critical fluid velocity, critical Reynolds number and critical Nusselt number were decreased.
- As the shell surface roughness to diameter ratio increases, the critical fluid velocity decreases and the pipe becomes instable at higher fluid velocities. In addition, with raising the shell surface roughness to diameter ratio, the critical Nusselt number decreases and consequently the heat transfer of the inside fluid was declined.

References

Ahouel, M., Houari, M.S.A., Bedia, E.A. and Tounsi, A. (2016), “Size-dependent mechanical behavior of functionally graded trigonometric shear deformable nanobeams including neutral surface position concept”, *Steel Compos. Struct., Int. J.*, **20**(5), 963-981.

Al-asadi, M.T., Mohammed, H.A., Kherbeet, A.Sh. and Al-aswadi, A.A. (2017), “Numerical study of assisting and opposing mixed convective nanofluid flows in an inclined circular pipe”, *Int. Commun. Heat Mass Transfer*, **85**, 81-91.

Amabili, M. (2008), *Nonlinear Vibrations and Stability of Shells and Plates*, Cambridge University Press.

Amabili, M., Karagiozis, K. and Païdoussis, M.P. (2009), “Effect of geometric imperfections on non-linear stability of circular cylindrical shells conveying fluid”, *Int. J. Non-Linear Mech.*, **44**(3), 276-289.

Anish, M., Kanimozhi, B., Ramachandran, S., Jayaprabakar, J. and Beemkumar, N. (2017), “Analysis of heat transfer through a high strength concrete with circular pipe in a safety vessel of reactor vault”, *Int. J. Amb. Energy*, **39**(7), 678-684.

Attia, A., Tounsi, A., Adda Bedia, E.A. and Mahmoud, S.R. (2015), “Free vibration analysis of functionally graded plates with temperature-dependent properties using various four variable refined plate theories”, *Steel Compos. Struct., Int. J.*, **18**(1), 187-212.

Bai, L., Lin, G. and Peterson, G.P. (2013), “Evaporative heat transfer analysis of a heat pipe with hybrid axial groove”, *J. Heat Transfer*, **135**, 031503 (9 pages).

Belabed, Z., Houari, M.S.A., Tounsi, A., Mahmoud, S.R. and Bég, O.A. (2014), “An efficient and simple higher order shear and normal deformation theory for functionally graded material (FGM) plates”, *Compos.: Part B*, **60**, 274-283.

Beldjelili, Y., Tounsi, A. and Mahmoud, S.R. (2016), “Hygro-thermo-mechanical bending of S-FGM plates resting on variable elastic foundations using a four-variable trigonometric plate theory”, *Smart Struct. Syst., Int. J.*, **18**(4), 755-786.

Belkorissat, I., Houari, M.S.A., Tounsi, A. and Hassan, S. (2015), “On vibration properties of functionally graded nano-plate using a new nonlocal refined four variable model”, *Steel Compos. Struct., Int. J.*, **18**(4), 1063-1081.

Bellifa, H., Benrahou, K.H., Hadji, L., Houari, M.S.A. and Tounsi, A. (2016), “Bending and free vibration analysis of functionally graded plates using a simple shear deformation theory and the concept the neutral surface position”, *J Braz. Soc. Mech. Sci. Eng.*, **38**(1), 265-275.

Bellifa, H., Benrahou, K.H., Bousahla, A.A., Tounsi, A. and Mahmoud, S.R. (2017), “A nonlocal zeroth-order shear deformation theory for nonlinear postbuckling of nanobeams”, *Struct. Eng. Mech., Int. J.*, **62**(6), 695-702.

Bennoun, M., Houari, M.S.A. and Tounsi, A. (2016), “A novel five variable refined plate theory for vibration analysis of functionally graded sandwich plates”, *Mech. Adv. Mater. Struct.*, **23**(4), 423-431.

Bessaim, A., Houari, M.S.A. and Tounsi, A. (2013), "A new higher-order shear and normal deformation theory for the static and free vibration analysis of sandwich plates with functionally graded isotropic face sheets", *J. Sandw. Struct. Mater.*, **15**(6), 671-703.

Besseghier, A., Houari, M.S.A., Tounsi, A. and Hassan, S. (2017), "Free vibration analysis of embedded nanosize FG plates using a new nonlocal trigonometric shear deformation theory", *Smart Struct. Syst., Int. J.*, **19**(6), 601-614.

Bouafia, Kh., Kaci, A., Houari M.S.A. and Tounsi, A. (2017), "A nonlocal quasi-3D theory for bending and free flexural vibration behaviors of functionally graded nanobeams", *Smart Struct. Syst., Int. J.*, **19**(2), 115-126.

Bouderba, B., Houari, M.S.A. and Tounsi, A. (2013), "Thermomechanical bending response of FGM thick plates resting on Winkler–Pasternak elastic foundations", *Steel Compos. Struct., Int. J.*, **14**(1), 85-104.

Bouderba, B., Houari, M.S.A., Tounsi, A. and Mahmoud, S.R. (2016), "Thermal stability of functionally graded sandwich plates using a simple shear deformation theory", *Struct. Eng. Mech., Int. J.*, **58**(3), 397-422.

Boukhari, A., Atmane, H.A., Tounsi, A., Adda Bedia, E.A. and Mahmoud, S.R. (2016), "An efficient shear deformation theory for wave propagation of functionally graded material plates", *Struct. Eng. Mech., Int. J.*, **57**(5), 837-859.

Buongiorno, J. (2006), "Convective transport in nanofluids", *J. Heat Transfer*, **128**, 240-250.

Bounouara, F., Benrahou, K.H., Belkorissat, I. and Tounsi, A. (2016), "A nonlocal zeroth-order shear deformation theory for free vibration of functionally graded nanoscale plates resting on elastic foundation", *Steel Compos. Struct., Int. J.*, **20**(2), 227-249.

Bourada, M., Kaci, A., Houari, M.S.A. and Tounsi, A. (2015), "A new simple shear and normal deformations theory for functionally graded beams", *Steel Compos. Struct., Int. J.*, **18**(2), 409-423.

Bousahla, A.A., Benyoucef, S., Tounsi, A. and Mahmoud, S.R. (2016a), "On thermal stability of plates with functionally graded coefficient of thermal expansion", *Struct. Eng. Mech., Int. J.*, **60**(2), 313-335.

Boylu, F., Dincer, H. and Atesok, G. (2004), "Effect of coal particle size distribution, volume fraction and rank on the rheology of coal–water slurries", *Fuel Process. Technol.*, **85**, 241-250.

Chica, J.A. and Morente, F. (2008), "A new model for transient heat transfer model on external steel elements", *Steel Compos. Struct., Int. J.*, **8**(3), 201-216.

Chikh, A., Tounsi, A., Hebali, H. and Mahmoud, S.R. (2017), "Thermal buckling analysis of cross-ply laminated plates using a simplified HSDT", *Smart Struct. Syst., Int. J.*, **19**(3), 289-297.

Colla, L., Fedele, L. and Buschmann, M.H. (2015), "Laminar mixed convection of TiO_2-water nanofluid in horizontal uniformly heated pipe flow", *Int. J. Therm. Sci.*, **97**, 26-40.

Chandel, S., Misal, R.D. and Beka, Y.G. (2012), "Convective Heat Transfer through Thick-Walled Pipe", *Proced. Eng.*, **38**, 405-411.

Chatterjee, S., Sugilal, G. and Prabhu, S.V. (2018), "Heat transfer in a partially filled rotating pipe with single phase flow", *Int. J. Therm. Sci.*, **125**, 132-141.

Ding, T., Cao, H.W., He, Zh.G. and Li, Zh. (2018), "Visualization experiment on boiling heat transfer and flow characteristics in separated heat pipe system", *Experiment. Therm. Fluid Sci.*, **91**, 423-431.

Draiche, K., Tounsi, A. and Mahmoud, S.R. (2016), "A refined theory with stretching effect for the flexure analysis of laminated composite plates", *Geomech. Eng., Int. J.*, **11**(5), 671-690.

El-Haina, F., Bakora, A., Bousahla, A.A. and Hassan, S. (2017), "A simple analytical approach for thermal buckling of thick functionally graded sandwich plates", *Struct. Eng. Mech., Int. J.*, **63**(5), 585-595.

Ezzat, M.A. and El-Bary, A.A. (2017), "A functionally graded magneto-thermoelastic half space with memory-dependent derivatives heat transfer", *Steel Compos. Struct., Int. J.*, **25**(2), 177-186.

Halelfadl, S., Estellé, P., Aladag, B., Doner, N. and Maré, T. (2013), "Viscosity of carbon nanotubes water-based nanofluids: Influence of concentration and temperature", *Int. J. Therm. Sci.*, **71**, 111-117.

Hussein, A.M. (2017), "Thermal performance and thermal properties of hybrid nanofluid laminar flow in a double pipe heat exchanger", *Experim. Therm. Fluid Sci.*, **88**, 37-45.

Kang, Sh.W., Wang, Y.Ch., Liu, Y.Ch. and Lo, H.M. (2017), "Visualization and thermal resistance measurements for a magnetic nanofluid pulsating heat pipe", *Appl. Therm. Eng.*, **126**, 1044-1050.

Khanafer, K. and Vafai, K. (2011), "A critical synthesis of thermophysical characteristics of nanofluids", *Int. J. Heat Mass Transfer*, **54**, 4410-4428.

Khetir, H., Bouiadjra, M.B., Houari, M.S.A., Tounsi, A. and Mahmoud, S.R. (2017), "A new nonlocal trigonometric shear deformation theory for thermal buckling analysis of embedded nanosize FG plates", *Struct. Eng. Mech., Int. J.*, **64**(4), 391-402.

Kim, I.G., Kim, K.M., Jeong, Y.Sh. and Bang, I.Ch. (2017), "Flow visualization and heat transfer performance of annular thermosyphon heat pipe", *Appl. Therm. Eng.*, **125**, 1456-1468.

Kolahchi, R., Safari, M. and Esmailpour, M. (2016), "Dynamic stability analysis of temperature-dependent functionally graded CNT-reinforced visco-plates resting on orthotropic elastomeric medium", *Compos. Struct.*, **150**, 255-265.

Larbi Chaht, F., Kaci, A., Houari, M.S.A. and Hassan, S. (2015), "Bending and buckling analyses of functionally graded material (FGM) size-dependent nanoscale beams including the thickness stretching effect", *Steel Compos. Struct., Int. J.*, **18**(2), 425-442.

Li, J. and Peterson, G.P. (2011), "3D heat transfer analysis in a loop heat pipe evaporator with a fully saturated wick", *Int. J. Heat Mass Transfer*, **54**, 564-574.

Li, Ch., Guan, Y., Wang, X., Li, G., Zhou, C. and Xun, Y. (2018), "Experimental and numerical studies on heat transfer characteristics of vertical deep-buried U-bend pipe to supply heat in buildings with geothermal energy", *Energy*, **142**, 689-701.

Maiga, S., Palm, S.J., Nguyen, C.T., Roy, G. and Galanis, N. (2005), "Heat transfer enhancement by using nanofluids in forced convection flows", *Int. J. Heat Fluid Flow*, **26**, 530-546.

Massoudi, M. and Johnson, G. (2000), "On the flow of a fluid particle mixture between two rotating cylinders, using the theory of interacting continua", *Int. J. Non-Linear Mech.*, **35**, 1045-1058.

Massoudi, M., Rajagopal, K.R. and Phuoc, T.X. (1999), "On the fully developed flow of a dense particulate mixture in a pipe", *Powd. Technol.*, **104**, 258-268.

Mahi, A., Bedia, E.A.A. and Tounsi, A. (2015), "A new hyperbolic shear deformation theory for bending and free vibration analysis of isotropic, functionally graded, sandwich and laminated composite plates", *Appl. Math. Model.*, **39**, 2489-2508.

Mehri, M., Asadi, H. and Wang, Q. (2016), "Buckling and vibration analysis of a pressurized CNT reinforced functionally graded truncated conical shell under an axial compression using HDQ method", *Comput. Meth. Appl. Mech. Eng.*, **303**, 75-100.

Menasria, A., Bouhadra, A., Tounsi, A. and Hassan, S. (2017), "A new and simple HSDT for thermal stability analysis of FG sandwich plates", *Steel Compos. Struct., Int. J.*, **25**(2), 157-175.

Meziane, M.A.A., Abdelaziz, H.H. and Tounsi, A.T. (2014), "An efficient and simple refined theory for buckling and free vibration of exponentially graded sandwich plates under various boundary conditions", *J. Sandw. Struct. Mater.*, **16**(3), 293-318.

Moradi-Dastjerdi, R. and Payganeh, Gh. (2017), "Transient heat transfer analysis of functionally graded CNT reinforced cylinders with various boundary conditions", *Steel Compos. Struct., Int. J.*, **24**(3), 359-367.

Mouffoki, A., Adda Bedia, E.A., Houari, M.S.A. and Hassan, S. (2017), "Vibration analysis of nonlocal advanced nanobeams in hygro-thermal environment using a new two-unknown trigonometric shear deformation beam theory", *Smart Struct. Syst., Int. J.*, **20**(3), 369-383.

Nguyen, C.T., Desgranges, F., Roy, G., Galanis, N., Mare, T., Boucher, S. and Angue Mintsa, H. (2007), "Temperature and particle-size dependent viscosity data for water-based nanofluids - Hysteresis phenomenon", *Int. J. Heat Fluid Flow*, **28**, 1492-1506.

Paak, M., Païdoussisn, M.P. and Misra, A.K. (2014), "Influence of steady viscous forces on the non-linear behaviour of cantilevered circular cylindrical shells conveying fluid", *Int. J. Non-Linear Mech.*, **58**, 167-183.

Reddy, J.N. (2002), *Mechanics of Laminated Composite Plates and Shells: Theory and Analysis*, Second Edition, CRC Press.

Saha, G. and Paul, M.C. (2017), "Transition of nanofluids flow in an inclined heated pipe", *Int. Commun. Heat Mass Transfer*, **82**, 49-62.

Sheikhzadeh, G.A., Teimouri, H. and Mahmoodi, M. (2013), "Numerical study of mixed convection of nanofluid in a concentric annulus with rotating inner cylinder", *Trans. Phenomen. Nano Micro Scales*, **1**, 26-36.

Shi, D.L. and Feng, X.Q. (2004), "The effect of nanotube waviness and agglomeration on the elastic property of carbon nanotube-reinforced composites", *J. Eng. Mater. Tech. ASME*, **126**, 250-270.

Shi, Ch., Wang, Y. and Xu, C. (2010), "Experimental study and analysis on heat transfer coefficient of radial heat pipe", *J. Therm. Sci.*, **19**, 425-429.

Sun, Y. and Zhang, X. (2015), "Heat transfer analysis of a circular pipe heated internally with a cyclic moving heat source", *Int. J. Therm. Sci.*, **90**, 279-289.

Vijayakumar, M., Navaneethakrishnan, P., Kumaresan, G. and Kamatchi, R. (2017), "A study on heat transfer characteristics of inclined copper sintered wick heat pipe using surfactant free CuO and Al2O3 nanofluids", *J. Taiwan Institut. Chem. Eng.*, **81**, 190-198.

White, F. (1986), *Fluid Mechanics*, McGraw-Hill, New York.

Zemri, A., Houari, M.S.A., Bousahla, A.A. and Tounsi, A. (2015), "A mechanical response of functionally graded nanoscale beam: an assessment of a refined nonlocal shear deformation theory beam theory", *Struct. Eng. Mech., Int. J.*, **54**(4), 693-710.

Zidi, M., Tounsi, A. and Bég, O.A. (2014), "Bending analysis of FGM plates under hygro-thermo-mechanical loading using a four variable refined plate theory", *Aerosp. Sci. Tech.*, **34**, 24-34.

CC